# High stability and activity of Pt electrocatalyst on atomic layer deposited metal oxide/nitrogen-doped graphene hybrid support

*Niancai Cheng [a], Jian Liu [a], Mohammad Norouzi Banis [a], Dongsheng Geng [a], Ruying Li [a], Siyu Ye [b], Shanna Knights [b], Xueliang Sun [a,*]*

[a] *Department of Mechanical and Materials Engineering, University of Western Ontario, London, ON N6A 5B9, Canada*
[b] *Ballard Power Systems Inc., 9000 Glenlyon Parkway, Burnaby, BC V5J 5J8, Canada*

## ARTICLE INFO

## ABSTRACT

A novel nanostructured support of $ZrO_2$/nitrogen-doped graphene nanosheets ($ZrO_2$/NGNs) hybrid was synthesized successfully by atomic layer deposition (ALD) technology to significantly improve the activity and stability of Pt electrocatalyst. Electrochemical test shows that Pt—$ZrO_2$/NGNs catalyst has 2.1 times higher activity towards methanol oxidation reaction (MOR) than Pt/NGNs catalyst, due to the promotion by $ZrO_2$ to the MOR on Pt surface. Pt—$ZrO_2$/NGNs catalyst has higher electrochemical surface area (ECSA) and better oxygen reduction reaction (ORR) activity than Pt/NGNs catalyst. Pt—$ZrO_2$/NGNs catalyst has also demonstrated 2.2 times higher durability than that of Pt/NGNs. The enhanced activity and durability were attributed to the unique triple-interaction of $ZrO_2$—Pt—NGNs. These findings indicate that metal oxide-metal-support is a promising catalyst structure for low temperature fuel cells.

## 1. Introduction

Proton exchange membrane fuel cells (PEMFCs) are regarded as ideal candidates for stationary and mobile power generation because of their high energy conversion efficiencies and low environmental impact [1,2]. However, the high cost and the poor durability of Pt-based electrocatalytic materials still remains a major obstacle for wide-spread commercialization of PEMFCs [3]. Currently, the porous carbon supported 2—5 nm Pt nanoparticles were usually used as anode and cathode catalysts in PEMFCs. However, the porous carbon support is not stable and it can be electrochemically oxidized in PEMFCs conditions, which results in Pt dissolution/agglomeration and carbon corrosion, and thus performance loss [4]. To address this challenge, much effort has been devoted to develop novel durable catalyst support materials such as graphitized carbon nanotubes (CNTs) [5,6], graphene [7], metal oxides, etc. [8—10].
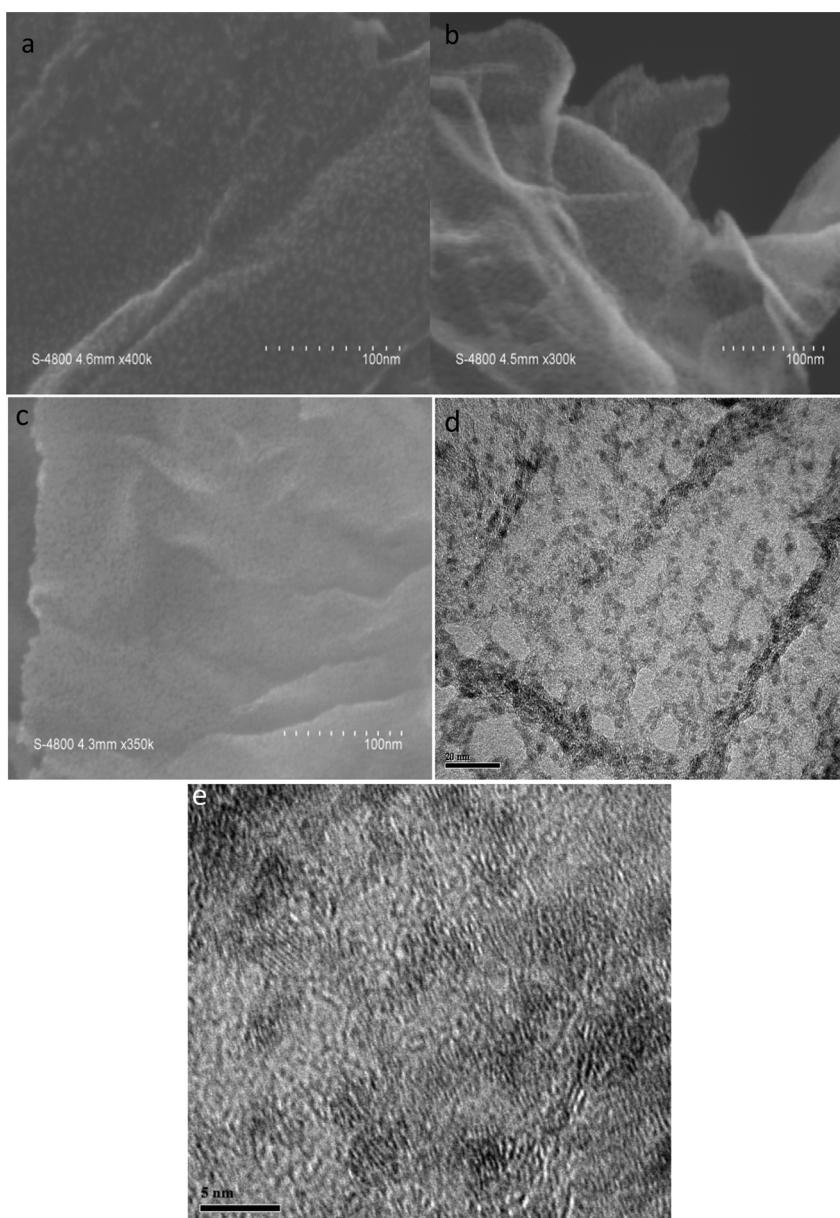
Recently, nitrogen-doped graphene has attracted a great attention as a unique 2D material with good conductivity, high surface area, and high mechanical strength, which are requirements of a good electrocatalyst support [11,12]. Heteroatom nitrogen-doping into graphene induces a change in spin density and charge distribution to the surrounding carbon

* *Corresponding author*. Tel.: +1 519 6612111x87759; fax: +1 519 6613020.
E-mail address: xsun@eng.uwo.ca (X. Sun).

atoms, resulting in the appearance of "activation regions" on the graphene surface [13,14]. This kind of "activation region" can participate in catalytic reactions, such as the oxygen reduction reaction (ORR). Furthermore, the nitrogen-doping can introduce disorder structures and defects on graphene, which can act as good anchoring sites for deposition of Pt nanoparticles [15,16]. Nitrogen-doping of graphene can increases the binding energy of Pt atom to the substrate [14] resulting in enhancement of the stability of Pt nanoparticles [12]. Nitrogen-doped graphene as a support has led to the improvement of Pt catalyst performance and stability, but further increase in activity and durability is still required.

In this work, we developed a $ZrO_2$/nitrogen-doped graphene nanosheets (NGNs) hybrid as a support to further enhance the performance and durability of Pt/NGNs catalyst through triple-interaction of Pt−$ZrO_2$−NGNs. Metal oxides with good catalytic properties and stronger interaction with Pt nanoparticles can generate active interfacial regions in the electrocatalysts and enhance the activity and stability of Pt catalysts [17−20]. The novel $ZrO_2$/NGNs hybrid support was prepared by growing $ZrO_2$ nanoparticles on NGNs using atomic layer deposition (ALD). Based on sequential and self-limiting surface reactions, ALD provides a powerful approach for the coating of ultra-fine metal oxides [21]. ALD technology can effectively control the size and distribution of metal oxides on substrate to create a proper interface structure between metal and substrate for Pt deposition. The Pt nanoparticles located and anchored at the interface of $ZrO_2$ and NGNs, which will improve the interaction of Pt with support by metal−metal oxide−NGNs junction. At the same time, this novel nano-structured catalyst can overcome the issues such as poor conductivity while only metal oxides support is used, because



**Fig. 1** − **SEM of ALD $ZrO_2$ on NGNs with (a) 5, (b) 10 and (c) 20 cycles at 250 °C. TEM (d) and HRTEM (e) of 5 ALD cycles $ZrO_2$ on NGNs at 250 °C.**
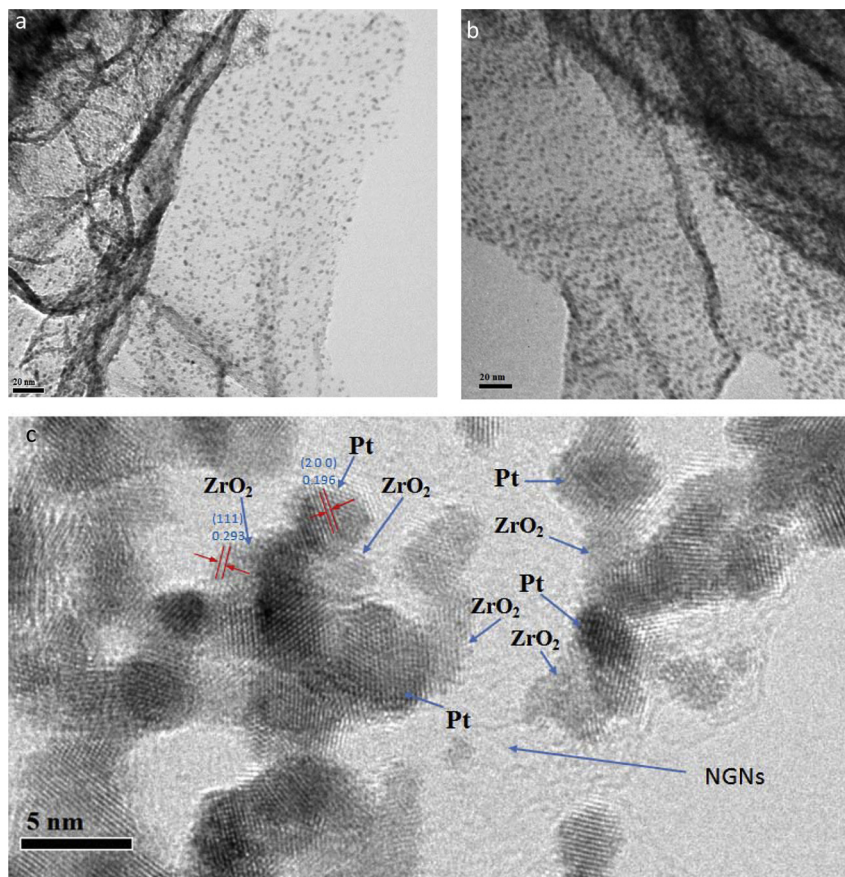
**Fig. 2 − TEM of (a) Pt/NGNs and (b) Pt−ZrO$_2$/NGNs. (c) HRTEM of Pt−ZrO$_2$/NGNs.**

Pt nanoparticle contact with metal oxide and NGNs at the interface of ZrO$_2$ and NGNs. These new catalyst materials were tested for potential application in PEMFCs, and they exhibited highly enhanced performance, and, particularly, durability due to this unique triple-interaction of ZrO$_2$−Pt−NGNs.

## 2. Methods

### 2.1. Synthesis of nitrogen-doped graphene nanosheets (NGNs)

Graphite oxide first was obtained by a modified Hummers methods previously reported by our group [22,23]. The received graphite oxide was then rapidly exfoliated via a thermal treatment at 1050 °C under Ar atmosphere yielding the product of graphene. NGNs were prepared by post heating the graphene under high purity ammonia mixed with Ar at 900 °C for 10 min.

### 2.2. Synthesis of ZrO$_2$/NGNs by ALD

The deposition of ZrO$_2$ on NGNs was carried out in an ALD reactor (Savannah 100, Cambridge Nanotechnology Inc., USA) at 250 °C using Zr(NMe$_2$)$_4$ and H$_2$O as precursors. Nitrogen gas was used as the carrier gas with a flow rate of 20 sccm. One ALD cycle was executed with the following six steps: (1) a

supply of Zr(NMe$_2$)$_4$ with a t1 (0.5 s) pulse time; (2) a 3.0 s extended exposure of Zr(NMe$_2$)$_4$ in the reaction chamber; (3) a purging of oversupplied Zr(NMe$_2$)$_4$ and any by-products with a t2 (30 s) purge time; (4) a supply of H$_2$O with a t3 (1 s) pulse time; (5) a 3.0 s extended exposure of H$_2$O to NGNs; (6) a
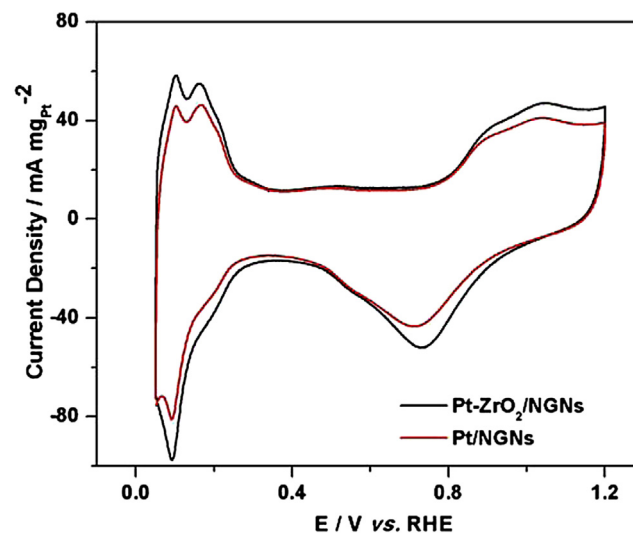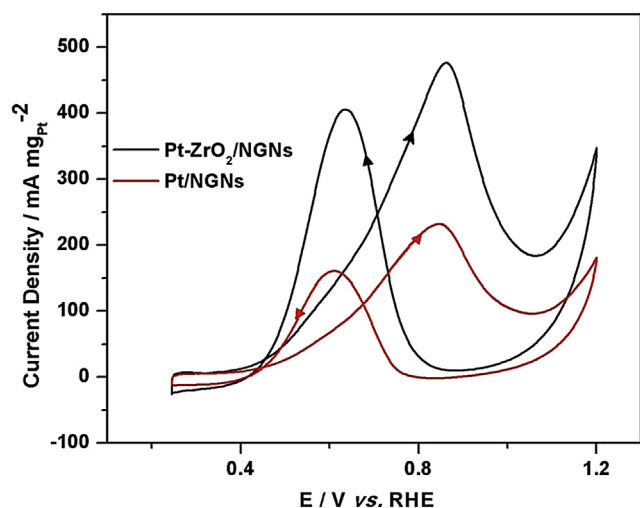


**Fig. 3 − Cyclic voltammograms of Pt−ZrO$_2$/NGNs and Pt/NGNs electrodes in 0.5 M H$_2$SO$_4$ solution at scan rate of 50 mV s$^{-1}$.**

**Fig. 4 – Cyclic voltammograms of Pt–ZrO$_2$/NGNs and Pt/ NGNs electrodes in 1 M CH$_3$OH + 0.5 M H$_2$SO$_4$ solution at scan rate of 50 mV s$^{-1}$.**

purging of excess H$_2$O and any by-products with a t4 (30 s) purge time. In short, the deposition procedure can be described as t1–t2–t3–t4. ZrO$_2$ was deposited on NGNs by repeating the above ALD cycle. More details have been previously reported by our group [24].

### 2.3. Synthesis of Pt/NGNs and Pt–ZrO$_2$/NGNs

Pt nanoparticles were deposited on the ZrO$_2$/NGNs hybrid support by ethylene glycol reduction method [17]. Briefly, the ZrO$_2$/NGNs in 50 ml ethylene glycol solution containing 0.2 mM H$_2$PtCl$_6$·6H$_2$O was sonicated for 10 min and then was refluxed at 160 °C for 3 h. After filtering and washing, the obtained catalyst was dried in a vacuum oven at 80 °C overnight. For comparison, Pt nanoparticles were also deposited on NGNs using the same procedure.

### 2.4. Materials characterization

The morphology and structure of samples were characterized by a field-emission scanning electron microscope (SEM, Hitachi S4800) equipped with energy dispersive X-ray spectroscopy (EDS), transmission electron microscope (TEM, Hitachi H7000) and high-resolution TEM (HRTEM, JEOL 2010FEG). The Pt loading on NGNs and ZrO$_2$/NGNs was confirmed by inductively coupled plasma-optical emission spectroscopy (ICP-OES). XANES measurements of Pt L3 edge were conducted on the 06ID superconducting wiggler sourced hard X-ray microanalysis (HXMA) beamline at the Canadian Light Source. The spectra were collected in fluorescence yield using a solid state detector, and the spectra of high purity metal Pt foil were collected in transmission mode for comparison and mono energy calibration.

### 2.5. Electrochemical characterization

The working electrodes were prepared with a procedure similar to the one reported previously [25]. Typically, the
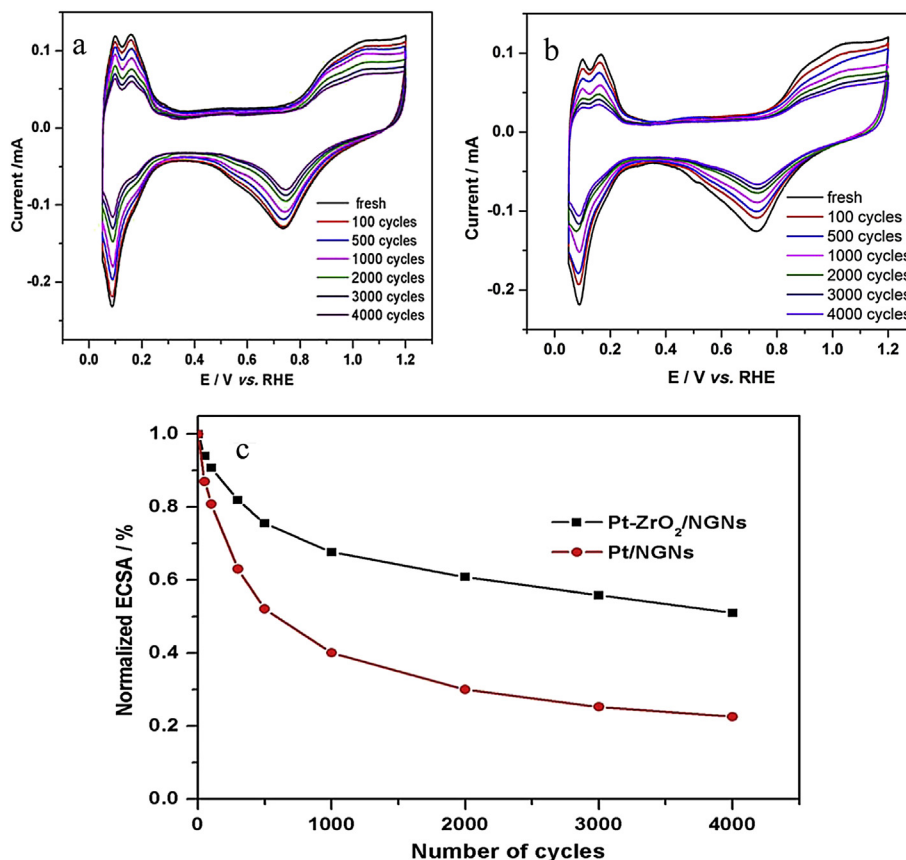
catalyst dispersions were prepared by mixing 5 mg of catalyst in 3 mL aqueous solution containing 1 mL of isopropyl alcohol and then ultrasonicated to form a uniform black ink. 10 μL of ink was pipetted on the electrode. After dying at room temperature, 5 μL of 0.05 wt% Nafion solution was applied onto the surface of the catalyst layer to form a layer protecting catalyst particles from detaching. A three-compartment cell was employed for the electrochemical measurements. A glassy carbon rotating-disk electrode (Pine Instruments) was used as the working electrode. Hg/Hg$_2$SO$_4$ electrode and platinum wire were used as the reference and the counter electrode, respectively. The potentials presented in this study are referred with respect to reversible hydrogen electrode (RHE). Before measurements, the working electrode was first activated with cyclic voltammetry (CV) (0.05–1.2 V, 50 mV s$^{-1}$) in a N$_2$-saturated 0.5 M H$_2$SO$_4$ solution until a steady CV was obtained. An oxygen reduction reaction (ORR) linear sweep voltammetry (LSV, 5 mV s$^{-1}$) was conducted in an O$_2$-saturated 0.5 M H$_2$SO$_4$ on the rotating-disk electrode system (Pine Instruments). Accelerated durability tests (ADT) were conducted by sweeping electrode potential between 0.6 and 1.2 V for 4000 cycles in O$_2$-saturated 0.5 M H$_2$SO$_4$. All the experiments were carried out at 25 °C.

## 3. Results and discussion

The morphology and structure of ALD ZrO$_2$ on NGNs support was shown in Fig. 1. SEM image of 5 cycles ALD ZrO$_2$ on NGNs indicated that ZrO$_2$ nanoparticles were formed on the surface of NGNs (Fig. 1(a)). Increasing in ALD cycles led to higher coverage of ZrO$_2$ on NGNs (Fig. 1(b) and (c)). 20 ALD cycles results in the formation of ZrO$_2$ film on the surface of NGNs, leaving no space on NGNs for deposition of other metals. This result shows ALD technology can be effectively used to adjust the size of ZrO$_2$ nanoparticles and coverage of ZrO$_2$ on NGNs surface to optimize the support hybrid structure for metal deposition. In this paper, 5 ALD cycles ZrO$_2$ coated on NGNs was used as hybrid support for Pt deposition. HRTEM was further used to investigate morphology and structure of 5 ALD cycle ZrO$_2$ on NGNs (Fig. 1(d) and (e)). Very uniform ZrO$_2$ nanoparticles with particle size of 2–4 nm were observed. 5 ALD cycles ZrO$_2$ coated NGNs should be suitable for depositing other metal nanoparticles on NGNs support to fabricate hybrid structure.

The Pt loading on NGNs and ZrO$_2$/NGNs were 21 wt% and 14 wt% respectively according ICP-OES. TEM images of Pt deposition on NGNs and ZrO$_2$/NGNs were shown in Fig. 2. The TEM image of Pt/NGNs (Fig. 2(a)) illustrates that the dispersion of Pt on NGNs is uniform and the averaged Pt nanoparticles size is 3.2 nm. Pt dispersion on ZrO$_2$/NGNs is also uniformly distributed, as shown in Fig. 2(c), with no indication of agglomeration and an average particle size of 3 nm. The HRTEM image reveals that the majority of Pt nanoparticles are located between the grain boundaries of ZrO$_2$ nanoparticles on NGNs in Fig. 2(c). TEM images (Fig. 2(b) and (c)) revealed the exact location of Pt and ZrO$_2$ nanoparticles on NGNs and that Pt–ZrO$_2$–NGNs hybrid nanostructure was formed.
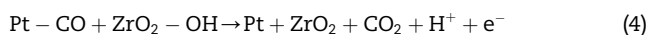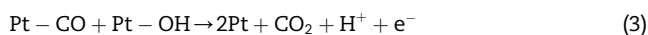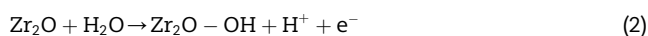
The cyclic voltammograms of Pt–ZrO$_2$/NGNs and Pt/NGNs in 0.5 M H$_2$SO$_4$ solution is displayed in Fig. 3. The typical hydrogen absorption/desorption peaks between 0.05 and 0.35 V, as well as well defined surface oxidation and reduction

Fig. 5 – Cyclic voltammograms for (a) Pt/NGNs and (b) Pt–ZrO$_2$/NGNs catalysts as function of the number of ADT cycles. (c) Normalized Pt ECSAs of Pt/NGNs and Pt–ZrO$_2$/NGNs catalysts as functions of ADT cycle number.

peaks, can be clearly observed. The electrochemical surface area (ECSA) of Pt is calculated from the charges of H$_2$ desorption peaks [25]. Pt–ZrO$_2$/NGNs catalyst has an ECSA of 65 m$^2$ g$^{-1}$, which is higher than the Pt/NGNs catalyst (48 m$^2$ g$^{-1}$). Pt-metal oxide interaction can promote OH removal on Pt surface by ZrO$_2$ nanoparticles [17], which is useful to improve Pt utilization.

As shown in Fig. 4, the activity of Pt catalyst towards methanol oxidation was improved by Pt–ZrO$_2$/NGNs hybrid nanostructure. The peak currents due to methanol oxidation in the forward scan for Pt–ZrO$_2$/NGNs and Pt/NGNs catalyst are 476 and 231 mA mg$^{-1}$Pt, respectively. The Pt–ZrO$_2$/NGNs catalyst displays 2.1 times higher current density than the Pt/NGNs. It is hypothesized that Pt–ZrO$_2$/NGNs hybrid nanostructure promotes the activity of Pt catalyst towards methanol oxidation according to the following reactions:

$$Pt + H_2O \rightarrow Pt - OH + H^+ + e^- \qquad (1)$$

$$Zr_2O + H_2O \rightarrow Zr_2O - OH + H^+ + e^- \qquad (2)$$

$$Pt - CO + Pt - OH \rightarrow 2Pt + CO_2 + H^+ + e^- \qquad (3)$$

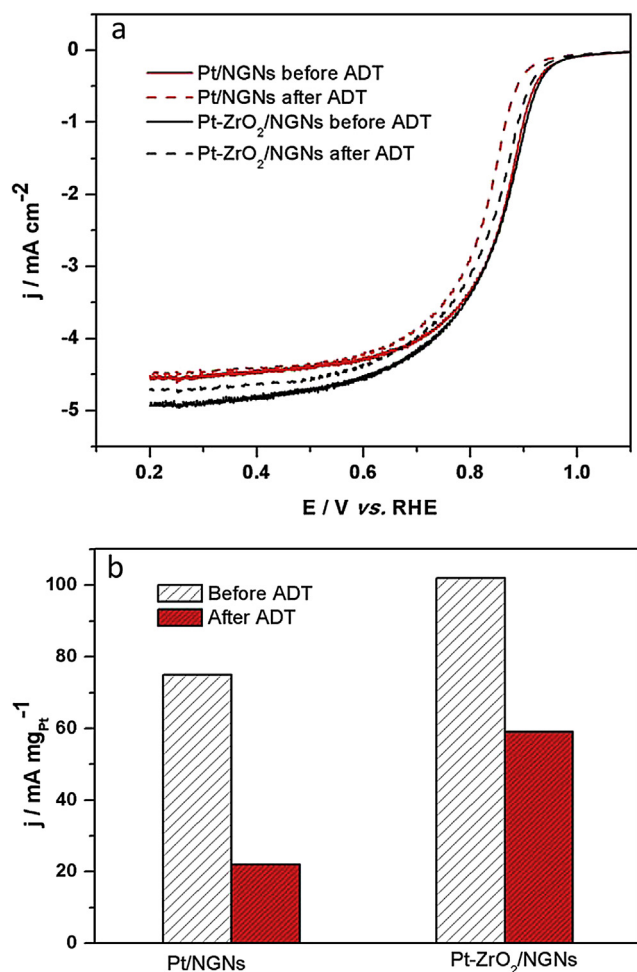$$Pt - CO + ZrO_2 - OH \rightarrow Pt + ZrO_2 + CO_2 + H^+ + e^- \qquad (4)$$

It is well known that a catalyst towards methanol oxidation need to break C–H and O–H bonds of methanol and facilitate

the reaction of the resulting residue with some O-containing species to form CO$_2$ [26]. During this reaction, some formed intermediates like CO species strongly adsorbed on Pt surface, which leads to self-poisoned Pt catalyst. The surface oxygen of a reducible oxide helps oxidizing the adsorbed CO on Pt surface [27]. So the enhancement of Pt–ZrO$_2$/NGNs towards methanol oxidation is likely to occur at the interface of Pt and ZrO$_2$ in the reaction (4).

The ADT results of both Pt/NGNs and Pt–ZrO$_2$/NGNs were investigated by sweeping electrode potential between 0.6 and 1.2 V for 4000 cycles in O$_2$-saturated 0.5 M H$_2$SO$_4$. As can be seen from Fig. 5(a) and (b), both catalysts exhibit a reduced activity in both hydrogen and oxygen regions with ADT cycles. The loss of electrochemical surface area (ECSA) was used to evaluate the catalyst activity loss with ADT cycles. The retained ECSA, normalized to the initial value, is plotted as a function of cycle number in Fig. 5(c). After 4000 cycles, about 23.5% of the initial ECSA of Pt/NGNs remains. In comparison, the Pt–ZrO$_2$/NGNs catalyst retains about 50.2% of the initial ECSA, which indicates that Pt–ZrO$_2$/NGNs catalyst has 2.2 times higher durability than Pt/NGNs catalyst. Pt on the ZrO$_2$/NGNs hybrid support is much more stable than that on NGNs under the same testing conditions.

Oxygen reduction reaction measurements were performed in O$_2$-saturated 0.5 M H$_2$SO$_4$ solution using a GC rotating-disk electrode at room temperature. Fig. 6 shows the ORR

Fig. 6 – (a) Polarization curves of Pt–ZrO$_2$/NGNs and Pt/NGNs for ORR before and after ADT cycles in O$_2$-saturated 0.5 M H$_2$SO$_4$ solution at room temperature. The potential scan rate was 5 mV s$^{-1}$ and the electrode rotation speed was 1600 rpm. (b) Stability characterization of Pt–ZrO$_2$/NGNs and Pt/NGNs at 0.9 V before and after ADT cycles.

that the catalytic activity of Pt catalysts toward ORR decreased. After 4000 cycles, Pt–ZrO$_2$/NGNs catalyst retains 59% of the initial value, while Pt/NGNs catalyst only keeps 28% (Fig. 6(b)). Therefore, Pt on ZrO$_2$/NGNs is more stable than NGNs under same test condition.

The enhanced durability is attributed to the ZrO$_2$–Pt–NGNs hybrid nanostructure: triple-interaction of ZrO$_2$–Pt–NGNs. Fig. 7 shows XANES spectra of Pt L3 edge of composite electrocatalysts. There is no significant change in the E0 of the Pt L3 edge for the composite samples compared to Pt foil, indicating the Pt metallic nature of the deposited catalysts. The absorption at 11 567 eV corresponds to 2p$_{3/2}$ to 5d transition, designated as the whiteline. The intensity of Pt L3 whiteline shows differences between the samples. The intensity of Pt L3 whiteline is a qualitative indicator of electron vacancies in the 5d orbitals of Pt atoms. The change in the whiteline intensity of the samples is as follows: Pt foil < Pt–ZrO$_2$/NGNs < Pt/NGNs. The decrease in whiteline intensity of Pt–ZrO$_2$/NGNs catalysts can be ascribed to the electron transfer resulting from the stronger metal support interactions (SMSIs) between Pt and ZrO$_2$–NGNs [5,30] compared with Pt/NGNs. During fuel cell operation, the corrosion of carbon support can take place at high potentials and can be accelerated by the promotion catalysis of Pt [31,32]. For Pt/NGNs, the Pt nanoparticles were anchored on the surface of NGNs just through the interaction of Pt–NGNs. For Pt–ZrO$_2$/NGNs catalyst, the Pt nanoparticles were anchored on the interface of ZrO$_2$ and NGNs through not only the interaction of Pt–NGNs and also the interaction of Pt–ZrO$_2$ (Fig. 2(c)). For Pt/NGNs catalyst, when the interaction of Pt–NGNs break because of carbon corrosion during fuel cell operation, the Pt nanoparticle will detach from the surface of NGNs or move in the electrode, result in the loss of Pt activity. For Pt–ZrO$_2$/NGNs catalyst, even though it lost Pt–NGNs interaction, the Pt nanoparticle is still anchored on the support through the interaction of Pt–ZrO$_2$. The ZrO$_2$–Pt–NGNs hybrid nanostructure thus enhances the Pt durability on the hybrid support. These findings indicate that metal oxide-metal-support is a promising catalyst structure for low temperature fuel cells. This unique triple-interaction of
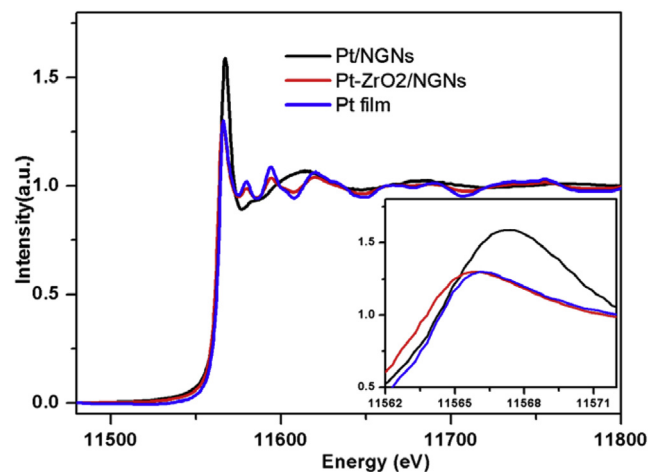
polarization curves for the Pt–ZrO$_2$/NGNs and Pt/NGNs catalysts. The polarization curves display the mixed kinetic–diffusion control region between ∼0.75 and ∼0.95 V, and the diffusion-limiting current region from ∼0.25 to ∼0.6 V. The kinetic current was calculated from the ORR polarization curves by using mass-transport correction and normalized to the loading amount of Pt, in order to compare the mass activity of different catalysts. According to the Levich–Koutecky equation [28]:

$$1/i = 1/i_k + 1/i_d$$

where i$_k$ is the kinetic current and i$_d$ is the diffusion-limiting current. It can be seen from Fig. 6(a), Pt/NGNs catalyst showed lower diffusion-limiting current than Pt–ZrO$_2$/NGNs. At 0.90 V, the ORR mass activities for Pt–ZrO$_2$/NGNs and Pt/NGNs catalysts are 102 and 78 mA mg$^{-1}$ respectively. It can be observed that the ORR curve shifts toward more negative potentials after 4000 cycles (Fig. 6(a)), which is consistent with previous observation on Pt catalyst [29]. The shifting means



Fig. 7 – XANES spectra of Pt L$_3$ edge of composite electrocatalysts.

$ZrO_2$—Pt—NGNs may be extended to study the structure and properties of other metal oxides - carbon supported catalyst materials.

## 4. Conclusion

$ZrO_2$/NGNs hybrid material was synthesized by ALD and is used as a support for Pt nanoparticles deposition. ALD can be effectively utilized to modify $ZrO_2$ nanoparticle size and coverage on NGNs in order to optimize parameters for Pt nanoparticle support. $ZrO_2$ nanoparticles on NGNs not only help improve Pt nanoparticles dispersion on NGNs, but also enhance the Pt activity towards ORR and MOR. The unique structure of $ZrO_2$/NGNs hybrid also enhances the Pt catalyst stability through triple-interaction of Pt—$ZrO_2$—NGNs. The Pt—$ZrO_2$/NGNs catalyst has 2.2 times higher durability than Pt/NGNs. This unique triple-interaction of metal oxide—metal—NGNs may be extended to study the structure and properties of other carbon-metal oxides supported catalyst materials.

## Acknowledgements

REFERENCES

[1] Escudero-Escribano M, Verdaguer-Casadevall A, Malacrida P, Grønbjerg U, Knudsen BP, Jepsen AK, et al. Pt5Gd as a highly active and stable catalyst for oxygen electroreduction. J Am Chem Soc 2012;134:16476—9.

[2] Wu Z-S, Yang S, Sun Y, Parvez K, Feng X, Müllen K. 3D nitrogen-doped graphene aerogel-supported $Fe_3O_4$ nanoparticles as efficient electrocatalysts for the oxygen reduction reaction. J Am Chem Soc 2012;134:9082—5.

[3] Zhang L, Li N, Gao F, Hou L, Xu Z. Insulin amyloid fibrils: an excellent platform for controlled synthesis of ultrathin superlong platinum nanowires with high electrocatalytic activity. J Am Chem Soc 2012;134:11326—9.

[4] Jiang ZZ, Wang ZB, Gu DM, Smotkin ES. Carbon riveted Pt/C catalyst with high stability prepared by in situ carbonized glucose. Chem Commun 2010;46:6998—7000.

[5] Ho VTT, Pan C-J, Rick J, Su W-N, Hwang B-J. Nanostructured $Ti_{0.7}Mo_{0.3}O_2$ support enhances electron transfer to Pt: high-performance catalyst for oxygen reduction reaction. J Am Chem Soc 2011;133:11716—24.

[6] Koenigsmann C, Santulli AC, Gong K, Vukmirovic MB, Zhou W-p, Sutter E, et al. Enhanced electrocatalytic performance of processed, ultrathin, supported Pd—Pt Core—shell nanowire catalysts for the oxygen reduction reaction. J Am Chem Soc 2011;133:9783—95.

[7] Antolini E. Graphene as a new carbon support for low-temperature fuel cell catalysts. Appl Catal B Environ 2012;123:52—68.

[8] Wang S, Yu D, Dai L. Polyelectrolyte functionalized carbon nanotubes as efficient metal-free electrocatalysts for oxygen reduction. J Am Chem Soc 2011;133:5182—5.

[9] Wang D, Yu Y, Xin HL, Hovden R, Ercius P, Mundy JA, et al. Tuning oxygen reduction reaction activity via controllable dealloying: a model study of ordered Cu3Pt/C intermetallic nanocatalysts. Nano Lett 2012;12:5230—8.

[10] Antolini E, Gonzalez ER. Ceramic materials as supports for low-temperature fuel cell catalysts. Solid State Ion 2009;180:746—63.

[11] Ignaszak A, Song CJ, Zhu WM, Zhang JJ, Bauer A, Baker R, et al. Titanium carbide and its core-shelled derivative TiC@$TiO_2$ as catalyst supports for proton exchange membrane fuel cells. Electrochim Acta 2012;69:397—405.

[12] He D, Jiang Y, Lv H, Pan M, Mu S. Nitrogen-doped reduced graphene oxide supports for noble metal catalysts with greatly enhanced activity and stability. Appl Catal B Environ 2013;132:379—88.

[13] Guo DJ, Qiu XP, Chen LQ, Zhu WT. Multi-walled carbon nanotubes modified by sulfated $TiO_2$-A promising support for Pt catalyst in a direct ethanol fuel cell. Carbon 2009;47:1680—5.

[14] Jia RL, Wang CY, Wang SM. Preparation of carbon supported platinum catalysts: role of pi sites on carbon support surface. J Mater Sci 2006;41:6881—8.

[15] Groves MN, Chan ASW, Malardier-Jugroot C, Jugroot M. Improving platinum catalyst binding energy to graphene through nitrogen doping. Chem Phys Lett 2009;481:214—9.

[16] Jafri RI, Rajalakshmi N, Ramaprabhu S. Nitrogen doped graphene nanoplatelets as catalyst support for oxygen reduction reaction in proton exchange membrane fuel cell. J Mater Chem 2010;20:7114—7.

[17] Chen YG, Wang JJ, Meng XB, Zhong Y, Li RY, Sun XL, et al. Atomic layer deposition assisted Pt-$SnO_2$ hybrid catalysts on nitrogen-doped CNTs with enhanced electrocatalytic activities for low temperature fuel cells. Int J Hydrogen Energy 2011;36:11085—92.

[18] Lv HF, Cheng NC, Peng T, Pan M, Mu SC. High stability platinum electrocatalysts with zirconia-carbon hybrid supports. J Mater Chem 2012;22:1135—41.

[19] Kou R, Shao Y, Mei D, Nie Z, Wang D, Wang C, et al. Stabilization of electrocatalytic metal nanoparticles at metal-metal oxide-graphene triple junction points. J Am Chem Soc 2011;133:2541—7.

[20] Xie H, Lu J, Shekhar M, Elam JW, Delgass WN, Ribeiro FH, et al. Synthesis of Na-stabilized nonporous t-$ZrO_2$ supports and Pt/t-$ZrO_2$ catalysts and application to water-gas-shift reaction. ACS Catal 2013;3:61—73.

[21] George SM. Atomic layer deposition: an overview. Chem Rev 2010;110:111—31.

[22] Geng D, Chen Y, Chen Y, Li Y, Li R, Sun X, et al. High oxygen-reduction activity and durability of nitrogen-doped graphene. Energy Environ Sci 2011;4:760—4.

[23] Kibsgaard J, Gorlin Y, Chen Z, Jaramillo TF. Meso-structured platinum thin films: active and stable electrocatalysts for the oxygen reduction reaction. J Am Chem Soc 2012;134:7758—65.

[24] Liu J, Meng X, Hu Y, Geng D, Banis MN, Cai M, et al. Controlled synthesis of zirconium oxide on graphene nanosheets by atomic layer deposition and its growth mechanism. Carbon 2013;52:74—82.

[25] Cheng N, Mu S, Pan M, Edwards PP. Improved lifetime of PEM fuel cell catalysts through polymer stabilization. Electrochem Commun 2009;11:1610—4.

[26] Frelink T, Visscher W, van Veen JAR. On the role of Ru and Sn as promotors of methanol electro-oxidation over Pt. Surf Sci 1995;335:353–60.

[27] Justin P, Hari Krishna Charan P, Ranga Rao G. High performance Pt–$Nb_2O_5$/C electrocatalysts for methanol electrooxidation in acidic media. Appl Catal B Environ 2010;100:510–5.

[28] Mayrhofer KJJ, Strmcnik D, Blizanac BB, Stamenkovic V, Arenz M, Markovic NM. Measurement of oxygen reduction activities via the rotating disc electrode method: from Pt model surfaces to carbon-supported high surface area catalysts. Electrochim Acta 2008;53:3181–8.

[29] Kou R, Shao Y, Wang D, Engelhard MH, Kwak JH, Wang J, et al. Enhanced activity and stability of Pt catalysts on functionalized graphene sheets for electrocatalytic oxygen reduction. Electrochem Commun 2009;11:954–7.

[30] Akalework NG, Pan CJ, Su WN, Rick J, Tsai MC, Lee JF, et al. Ultrathin $TiO_2$-coated MWCNTs with excellent conductivity and SMSI nature as Pt catalyst support for oxygen reduction reaction in PEMFCs. J Mater Chem 2012;22:20977–85.

[31] Roen LM, Paik CH, Jarvic TD. Electrocatalytic corrosion of carbon support in PEMFC cathodes. Electrochem Solid State Lett 2004;7:A19–22.

[32] Siroma Z, Ishii K, Yasuda K, Miyazaki Y, Inaba M, Tasaka A. Imaging of highly oriented pyrolytic graphite corrosion accelerated by Pt particles. Electrochem Commun 2005;7:1153–6.